Hindawi
Journal of Food Quality
Volume 2024, Article ID 9874786, 1 page
https://doi.org/10.1155/2024/9874786

Retraction

Retracted: Multisensor Data and Cross-Validation Technique for Merging Temporal Images for the Agricultural Performance Monitoring System

Journal of Food Quality

Received 23 January 2024; Accepted 23 January 2024; Published 24 January 2024

This article has been retracted by Hindawi following an investigation undertaken by the publisher [1]. This investigation has uncovered evidence of one or more of the following indicators of systematic manipulation of the publication process:

(1) Discrepancies in scope

(2) Discrepancies in the description of the research reported

(3) Discrepancies between the availability of data and the research described

(4) Inappropriate citations

(5) Incoherent, meaningless and/or irrelevant content included in the article

(6) Manipulated or compromised peer review

The presence of these indicators undermines our confidence in the integrity of the article's content and we cannot, therefore, vouch for its reliability. Please note that this notice is intended solely to alert readers that the content of this article is unreliable. We have not investigated whether authors were aware of or involved in the systematic manipulation of the publication process.

Wiley and Hindawi regrets that the usual quality checks did not identify these issues before publication and have since put additional measures in place to safeguard research integrity.

We wish to credit our own Research Integrity and Research Publishing teams and anonymous and named external researchers and research integrity experts for contributing to this investigation.

The corresponding author, as the representative of all authors, has been given the opportunity to register their agreement or disagreement to this retraction. We have kept a record of any response received.

References

[1] V. K. S. Maddala, K. Jayarajan, M. Braveen et al., "Multisensor Data and Cross-Validation Technique for Merging Temporal Images for the Agricultural Performance Monitoring System," *Journal of Food Quality*, vol. 2022, Article ID 9575423, 10 pages, 2022.

Hindawi
Journal of Food Quality
Volume 2022, Article ID 9575423, 10 pages
https://doi.org/10.1155/2022/9575423

Research Article

Multisensor Data and Cross-Validation Technique for Merging Temporal Images for the Agricultural Performance Monitoring System

Venkata Kanaka Srivani Maddala,[1] **K. Jayarajan**,[2] **M. Braveen**,[3] **Ranjan Walia**,[4] **Patteti Krishna**,[5] **Sivakumar Ponnusamy**,[6] **and Karthikeyan Kaliyaperumal**[7]

[1]*Department of Science and Humanities, Vignans Foundation for Science Technology and Research Deemed to Be University, Vadlamudi Guntur District, Guntur 522213, Andhra Pradesh, India*
[2]*Department of Information Technology, Malla Reddy Engineering College for Women, Secunderabad, Telangana 500100, India*
[3]*School of Computer Science and Engineering, Vellore Institute of Technology, Chennai 600127, India*
[4]*Department of Electrical Engineering, Model Institute of Engineering and Technology, Jammu, Jammu & Kashmir 181122, India*
[5]*Department of Electronics and Communication Engineering, Netaji Subhas University of Technology East Campus (Formerly AIACTR), Geeta Colony, New Delhi-110031, India*
[6]*Department of Computer Science and Engineering, SRM Institute of Science & Technology, Delhi NCR Campus, Modinagar, Ghaziabad, Uttar Pradesh 201204, India*
[7]*IoT—HH Campus, Ambo University, Ambo, Ethiopia*

Correspondence should be addressed to Karthikeyan Kaliyaperumal; karthikeyan@ambou.edu.et

Received 4 February 2022; Accepted 8 March 2022; Published 1 April 2022

Academic Editor: Rijwan Khan

Many approaches for crop yield prediction were analyzed by countries using remote sensing data, but the information obtained was less successful due to insufficient data gathered due to climatic variables and poor image resolution. As a result, current crop yield estimation methods are obsolete and no longer useful. Several attempts have been made to overcome these difficulties by combining high precision remote sensing images. Furthermore, such remote sensing-based working models are better suited to extraterrestrial farmers and homogeneous agricultural areas. The development of this innovative framework was prompted by a scarcity of high-quality satellite imagery. This intelligent strategy is based on a new theoretical framework that employs the energy equation to improve crop yield predictions. This method was used to collect input from multiple farmers in order to validate the observation. The proposed technique's excellent reliability on crop yield prediction is compared and contrasted between crop yield prediction and actual production in different areas, and meaningful observations are provided.

1. Introduction

The agricultural sector accounted for nearly 30% of the land surface, with only about 12 percent dedicated to crop production and the remainder serving as cattle pasture. Agriculture is experiencing unprecedented pressures as a result of the rapid growth of the world's population [1]. The agricultural field faces unique challenges that are rarely met and that vary depending on the socioeconomic area in which the farmer lives. Natural geography, weather conditions, and agricultural practices are all factors that influence grain production. Each of these variables differed significantly across geographic and temporal boundaries [2]. According to this report by the Food and Agriculture Organization of the United Nations (FAO) [3], there is still a need for timely agricultural information as well as an effective monitoring mechanism in order to improve crop yield. It was discovered that remote sensing technology was well suited for collecting

data across large agricultural areas at frequent intervals with less time and that remote sensing technology may make a significant contribution toward providing a fast comprehensive image [4]. Remote sensing images are important for the farm administration because their exceptional capability can represent the conditions of crop development both geographically and chronologically. Crop growth, photosynthetic rate, plant management, or water levels can be easily predicted and measured [5–8].

Many methods of converting remote sensing information into agricultural outputs have been favoured, while many evaluations of these methods exist [9]. Many of these methods had encountered problems during the calculation of crop production. One such issue was the lack of adequate remote sensing information on agricultural fields due to weather conditions. Several efforts have been made to overcome these problems, including an example which the technique described [10], by substitution of low quality images with high temporal methods. Two primary challenges which prohibit the crop yield rate were less quality images with inadequate sequential accuracy rate of the crop condition due to the cloud interference while capturing the images [11]. Few researchers have worked on calculating crop output through its yield indices [12] and noted the two main constraints. Primary expenditure incurred for the collection of all relevant inputs and topographic maps in certain situations. This may indeed be the reliability of the study with existing methods of predicting crop yield.

2. Materials and Methods

Scientists used satellite pictures to estimate crop yield from farm levels [13]. They preferred vegetation indices as a parameter and measured the production rate through satellite images. The results showed a very weak link between vegetation indexes on crop yield prediction and R 0.52 observations. The main reason for this observation is that the crop has been covered with water for a long time and the proposed method is therefore absolute [14]. Using the nonlinear correlation technique considering parameters such as soils, water, vegetation indices, and climatic temperatures, crop yield rate of Kansas region from the United States for a period of 20 years on agricultural production were computed and forecast. This regression technique enables production deviations and forecast errors to be reduced to a greater extent. This method was perfectly suited to large agricultural areas which produce homogeneous agricultural products.

In [15], Montecito's approach was employed to compute the photosynthesis activity of the crop and Auburn's approach was used to determine the effectiveness of the sunlight fall through Surfaces Energetic Balancing Algorithms of Soil (SEBAL) method. This method accounts for temporal and geographic variations in soil conditions. The production rate ranges from 1100 to 1300 kg/ha relative to the expected and actual yield of the crop. This was because of the available data and the information that feeds the demand for SEBAL on global weather conditions [16]. To compute the actual evaporation rate, our approach relies more on weather data. A further innovative theoretical framework has been added to the developed Monod framework. For this new method of estimation of agricultural production, algorithms, methods, and remote sensing information were used. This method will create a new conceptual framework that takes into account the lack of available information caused by environmental variables.

3. Techniques and Data Type

Various cultivation techniques and environmental factors distinguish farmers across various nations. Such variety adds towards overall difficulty for addressing an issue with agricultural prediction. The researchers must seek out any single answer which could adjust with changing weather circumstances and measure the overall accessibility of the crop field through remote sensing data.

The research location for the present study is Lebanon's largest agricultural region, namely, the Bekaa Valley (Figure 1). The agricultural area extends over an area of 1250 km. The primary yield in this area was rice and wheat. The climate station has been installed in two regions and provides information on weather and crop yield conditions. The measurement from the data centre shows that almost the entire measurements of the climates were found to be identical and the yield rate was also found to be the same on the regions. Only one weather station deployed on a large agricultural area was comparable and the information obtained will be sufficient to predict agricultural performance, because the region has a uniform climate and the homogeneous cultivation of the crops makes the study compact.

In addition, the available satellite images based on thermal radiation from the culture field provide excellent geographic information. The ultraviolet spectrum is at 60 m against 1,000 m for the MODIS satellite. In this case, the long-distance thermal spectrum was used to measure the forecast of agricultural output. It was originally planted or harvested. The combination of latitudes 9 and 10 makes it possible to improve the image quality and, consequently, the measuring days have been reduced from 16 to 10 days.

The Monod concept [17] was built upon this photosynthesis radiation measurement (PAR) (universal set mm). The measurement was taken into consideration by the photosynthesis process and the amount of respiration occurred during vegetation. The amount of sunlight used to develop the photosynthesis process was taken into account. According to [18], about 45–50% of energy was consumed and it was commonly used to measure overall performance over a 24-hour period:

$$\text{photo active radiation} = 0 : 24 L_i . \tag{1}$$

Consequently, the PAR represents only a tiny part of the total solar light received. The whole crop in the field absorbs a small amount of light for photosynthesis. The equation PAR shown below can be used to compute chlorophyll uptake activity.

$$\begin{aligned} &\text{Absorbed photo active radiation} \\ &= t * \text{factor of photo active radiation.} \end{aligned} \tag{2}$$

Figure 1: Area of research.

As stated in [19], this variable t could be calculated using the PAR which was measured using the vegetation index, where

$$t = 0 : 182 \,|\, 2.258 * \text{normalized differences vegetation index}. \tag{3}$$

The Normalized Differences Vegetation Index is generally calculated by dividing its difference between the actual spectra received. Based on this modified Jones theory, biomass accumulation in the region will be equal to cumulative PAR.

$$\text{Biomass} = \sum \text{absorbed PAR}\ (p)\,(p), \tag{4}$$

where p represents the period.

This process did not require any additional information on a particular type of crop. Cereals, millet, hay, grasslands, or potatoes may be produced and reported. There are significant impacts from this approach. The chlorophyll plants could be converted using that exact approach. Formula (5) shows the sunlight usages, as this equation was largely acceptable for the measurement of the effective use of sunlight [20]:

$$\text{efficiency} = p_1 p_2 F. \tag{5}$$

Whenever climatic conditions are ideal, their maximum conversion factor occurs below the surface of the plate (at the root section) and the measure was equal to 1.37 g/MJ. An optimum percentage of soil state was measured by F.

Groundwater absorbers are primarily determined by the evaporation rate of the root layer. The complete F calculation process is further detailed.

$$\begin{aligned} p_1 &= 0.6 + 0.03\text{temp}_{\text{air}} - 0.004\left(\text{temp}_{\text{air}}\right)^2, \\ p_2 &= \frac{1}{1 + \exp\left(0.03\text{temp}_{\text{air}} - 8 - \text{temp}_{\text{monthly}}\right)} \\ &\quad \times \frac{1}{\exp\left(0.03\text{temp}_{\text{air}} - 8 - \text{temp}_{\text{monthly}}\right)}. \end{aligned} \tag{6}$$

P1 and P2 are the separate heater characteristics. The average airflow was measured at the culture condition where it was exposed with more leaves. The monthly airflow was measured on the airflow per day. From the equations it was clear to infer that P1 depend on the mean air flow rate and P2 depend on both the mean and the monthly air flow rate. This mentioned information can be acquired either by installation of the local climate measurement station as stated in the literature or through the remote sensing images from the local satellites by complicated statistical techniques to predict the crop production rate.

When using the latitude satellite outputs, problems such as the image without information and the corrections of the scanner's line concealer are noted. Usually, the information is referenced and includes all spot images saved day by day. The images will include information gaps, as they are all acquired through identical metrology and geometric adjustments. These corrected images may contain errors and the data gathered via the SLC system may malfunction. To solve this problem, [21] designed mechanism followed by filling the blanks part of the images with the nearly same image obtained through the satellite image. GIS technology has been used in the input preprocessing phase [22]. With

such an approach, the overall picture was adjusted using quadratic transformation as a function of both normal variation and average frequencies at each zone [23].

$$\text{Reflectance} = \text{band specific} + \text{calibrated quantized} + \text{band}. \quad (7)$$

Band variables are taken from color information that arrived from each picture. These picture pixel counts are used to calculate the overall Calibrated quantized score. This technique was used to help adjust transfer functions with position purple color current sunlight.

$$\begin{aligned}
\text{Reflectance} &= \frac{(\text{reflectance})'}{\sin\theta},\\
\text{reflectance} &= \frac{\text{reflectance} - Z(1 - \text{band})}{\text{quantized band}},\\
\text{narrow transmit input} &= Z_1 \exp\left[\frac{Z_2 \times \text{air} - \text{pressure}}{\text{clearness of Sin}\,\theta}\right] + Z_5,\\
\text{narrow transmit output} &= Z_1 \exp\left[\frac{Z_2 \times \text{air} - \text{pressure}}{\text{clearness of Cos}\,\theta}\right] + Z_5,\\
\text{work} &= 0.14 \times \text{air} - \text{pressure} + 2.1,\\
\text{actual pressure} &= \frac{\text{relative humidity}}{100},\\
\text{saturated pressure} &= 0.61 \times \exp\left(\frac{17.27\,\text{temp}_{\text{air}}}{\text{temp}_{\text{air}} + 237.2}\right),\\
\text{air} - \text{pressure} &= 102.2\left(\frac{365 - 0.0032c}{365}\right)^2.
\end{aligned} \quad (8)$$

Equation (9) was used to calculate this evaporation fraction, which was dependent on the total power imbalance equation (10).

$$\text{Evaporative fraction} = \frac{\alpha(\text{factor})}{\text{net radiation} - \text{soil heat flux}}, \quad (9)$$

$$\alpha(\text{factor}) - \text{net radiation} - \text{soil heat flux} - \text{sensible heat flux}. \quad (10)$$

The overall energy imbalance was calculated using remote sensing images that typically provide geographic data for a very large region, including data on energy output and water content.

In this work, observations are computed using both evaporation percentages and real-time evaporation perspiration. These were compared to their calculation based on actual data collected from the data centre [24]. SEBAL includes measuring principles, concepts, and procedures. Measurements are computed on each individual parameter resulting in total irradiation using the following equations:

$$\begin{aligned}
\text{net radiation} &= \text{short wave radiation} - \text{surface}\,(\text{short wave radiation}) - \text{longwave radiation}\\
&\quad - (1 - \text{thermal sensitivity}),
\end{aligned} \quad (11)$$

$$\text{sensible heat flux} = \text{density of air} \times \text{heat capacity}\,\frac{(\text{temp}_{\text{air}} - \text{temp}_{\text{surface}})}{\text{transfer resistance}}, \quad (12)$$

$$\text{soil heat flux}\,(0.05 + 0.10\ \text{of factor})Rn, \quad (13)$$

$$\text{soil heat flux} = \text{maximum}\,(0.4 \times \text{sensible heat flux},\ 0.15Rn). \quad (14)$$

4. Development of a Mathematical Model

The study had limited forecast of agricultural output because it was based on a limited number of satellite images. There are regular delays between crop dates and this incomplete picture results in poor forecasting of crop yield. To make it available and acceptable, the mathematical model was designed to compensate for the problem [25]. The developed statistical model will compensate for any lack in image during the growth of the crop and all images will be used for the mathematical prediction of crop yield.

Therefore, an attempt was made to anticipate effectiveness, and statistical methods were used to assess observations from reality, including satellite photographs. With this case, they are implemented to help improve the accessibility of knowledge to crop forecasting with a specific

specialized informational workflow such as bioenergy estimation. Its interpolation of blank information using the known entry aimed at achieving the least possible loss.

Information derived from satellite images, another hand of information, provides growth of particular crops and therefore becomes a relatively complex nonpolynomial problem. Therefore, a reliable approach was taken to effectively resolve the situation to provide the optimal solution.

The objective was to use a mathematical optimisation technique as a nonlinear optimisation technique to obtain a curve adapted to crop yield detection information. The techniques are based on the selected regions because the information obtained by remote sensing will provide accurate information on the test area and this will reduce complications. The basic concept was that the linear function used another smaller functional Qu which accurately represents the functional activity F inside the test area Nn at the test location x. An additional test was calculated by minimizing R (minimum Q(s), s N) on the test area considered. It is referred to as the test region section and the trusted region thread was generally represented as

$$\text{minimum}\left\{\frac{1}{2}r + \text{gradient of diagonal}\right\}. \tag{15}$$

The modified Jones method was used calculate the biomass statistics from a single satellite picture; this same bioenergy information was gathered for all days for a calendar year. Then all pictures are employed to the optimisation procedure that develops a new statistical framework.

Finally, new biomass energy is derived from (16), which can be used to calculate the overall crop yield from the first growing period until harvest.

$$\text{Estimated biomass} = \sum_{j=1}^{M} \text{mathematical of available Landsat image.} \tag{16}$$

This new technique has the advantage of being able to further represent the growth phases of the entire culture, despite the absence of some informative images available. Our involved procedures construct this model with the help of a few satellite photos and the process involved is elaborated in detail in Figure 2.

5. System Development

Policy makers, researchers, and farmers need a reliable method to properly predict agricultural production. The proposed platform must always be accessible at all times, which implies nothing with environmental conditions and should likely provide valuable information to applicants.

This intelligent network was usually built up from many parts which work together to achieve some certain goal. The system developed would be capable of taking decisions and then carrying out specific activities on the basis of those decisions. This underlying component to every intelligence system with many functions that perform is described in its subsequent architecture and is shown in Figure 3. This smart technology can simply be a very preliminary approach to predicting crop yields among different crop types. The participation of all products within an intelligent system will be key to the overall effectiveness of the framework. This intelligent system begins with various activities through the acquisition of information components and the verification of safety information and its effectiveness, as shown in Figure 4.

In addition, the use of this smart framework that was built on availability data showed improved efficiency. Ultimately, the crop yield rate or the estimation can be measured either through the developed method or in a direct way based on the availability of the data as shown in Table 1.

6. Experimental Results

The experiments were carried out in accordance with the nature of the information, the agricultural product, and the total duration of the study. Despite the fact that farming is in full swing, if not all of the necessary information is available, intelligence systems can be used to assess crop yield performance. The current research has been restricted to the rate of seed potato production over a period of three distinct phases, which has been the focus of the previous work. During the winter, the crop will be planted and harvested, and the crop will be harvested and harvested again during the middle of the summer season. Within 20 days of sowing the potato seeds, the young potato leaves are ready to harvest and eat. Cloud disruptions will occur during the test reaction during this season, and it is the cloud season that has the potential to degrade the quality of the satellite image.

Overall, 8 series of images are captured between these two seasons for crop yield prediction. In the trial weeks of March and late August, some photos were taken after planting the potatoes (15–25 weeks later). The growing season of the study crop will take approximately 25–35 weeks prior to collection and the observations are presented in Tables 2 and 3. As stated earlier if there are any errors in the images, the latitude 8 satellite was adjusted using the change of bands and the new images are captured. Furthermore, environmental adjustments were made in the images taking into account surface reflection when capturing the images. Thus, self-improvement images and self-reflection have been taken into account.

6.1. Calculation. The measurement system is used to calculate the percentage of evaporation on real time. The images are taken each month from April until July, with the

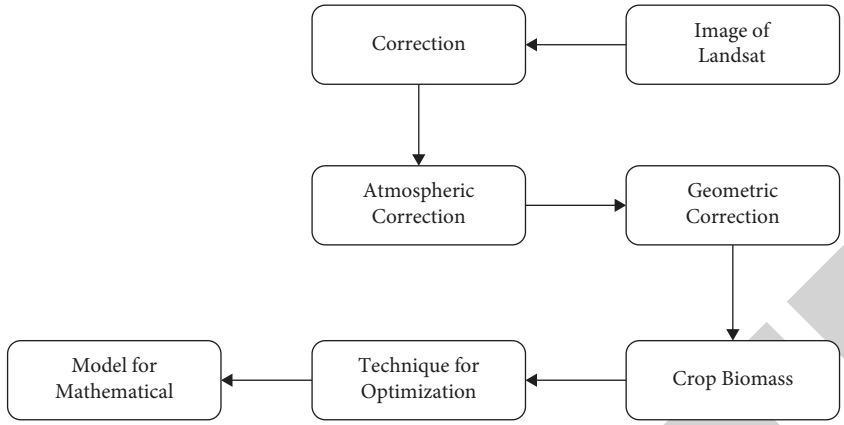

Figure 2: The newly developed mathematical model.

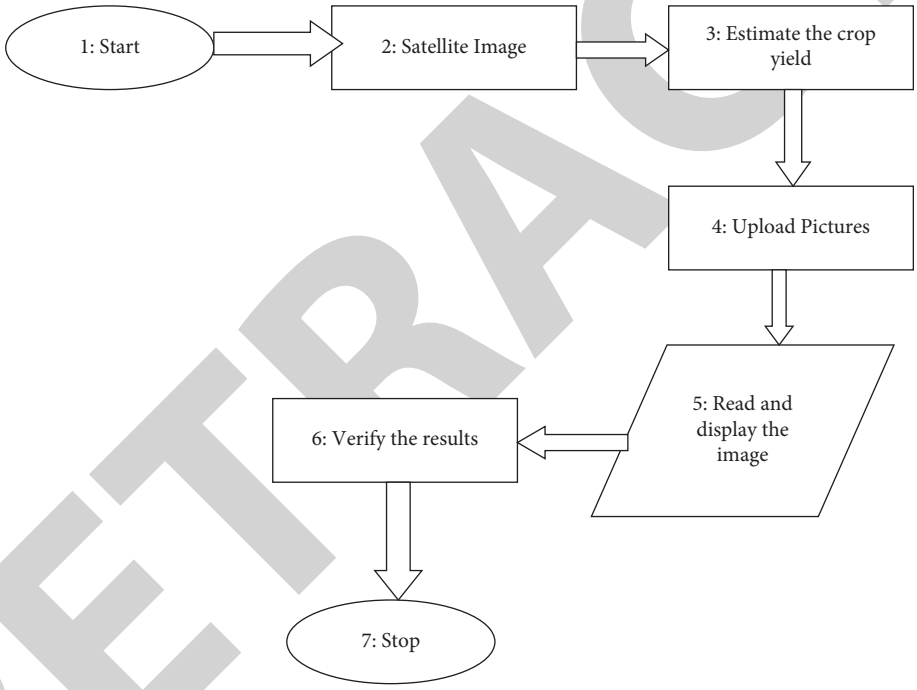

Figure 3: Crop production estimation using an intelligent system.

exception of the relatively selected cases where total irradiation was extremely important in relation to the surface temperature rate ($Rn >> H$ and $Rn >> G0$). D was zero because near-ground temperatures were almost identical or observation variations could be low. After that, the percentage of evaporation will typically be less than 1. All climate data collected at the data collection centre sites were used to estimate actual evaporation relative to the percentage of evaporation recorded. The gathered satellite images will enhance the overall accuracy of the system layer technique. Representation of satellite images and actual evaporation rates include evaporation maps over a vast region of the test region.

The actual evaporation rates collected by the data centre point (actual numbers) with respect to the two projected observations were compared to measure the efficiency of the proposed model. The error component was measured through the calculation of the mean absolute error (MAE). The data is taken during the month of April 2020 in the morning session to measure the evaporation percentage values. Its actual percentage difference was 5%, when this projected $Wm = 0.74$ was calculated using an elaborate mathematical model and is compared to the data station at about the same time.

These findings from an evaporation rate calculated on June 29, 2020, were fully measured and documented. The parameters of the energy balance equation are used and the data from the data centre are compared, as shown in Table 3. The calculations show different parameter information which is obtained by the data centre located in the test area.

Figure 4: Bekaa Valley transpiration maps.

Table 1: Calculation of remote sense and Bowen ratio.

Day	Location	Bowen ratio	Remote sense	Defect
1	Elias	3.26	3.2	7.5
2	Tanay	2.29	4.2	8
3	Elias	4.16	3.44	8.5
4	Tanay	3.26	2.9	6

Table 2: Using energy balance, we calculate the evaporative percentage for April 2020.

Period	Ratio	Humidity	Flux heat of latent	Fraction of evaporation
10.30	117	9.36	110.06	0.36
12.00	326	23.26	225.03	0.38
13.30	507	66.2	320.23	0.42
15.00	389	52.3	312.65	0.40

Table 3: Using energy balance, wecalculate the evaporative percentage for August 2020.

Period	Ratio	Humidity	Flux heat of latent	Fraction of evaporation
10.30	340	10.26	236.36	0.36
12.00	286	16.29	207.26	0.49
13.30	364	26.27	218.67	0.46
15.00	5026	32.2	349.79	0.42

An evaporation ratio V is calculated from the collected information and has been compared to the developed model. The error rate was up to 8%. These results were encouraging and explain that the derivative V using this model approach has a good level of reliability. Based on the observation, we can conclude that the proposed calculation will address the issue raised during remote sensing technology.

6.2. Crop Yield Estimation. The remote sensing data are collected through the latitude 9 satellite. The series of 8 images is collected to calculate potato output. However, the effects of bioenergy on crop development phase data, the overall amount of images collected, and temporal coverage are great. This greatly reduces the quality of the data and renders it insufficient. This could be handled successfully by getting the everyday picture by drones or other modes. However, the quality of the picture significantly determines the quality of the efficiency of the model. The data collected will remain worthless because most drones or other satellites have provided poor spatial images, especially with heat and ultrasonic factor considerations. These issues can be resolved using the developed model, and any mathematical framework can be used to address them.

Information sets are collected from potato records and maps have been generated from all satellite images analyzed. Figure 5 shows the lowest, highest, and average biomass output of individual potato farms according to these images. Although April potato planting times vary with planting, overall, most farmers start planting in early April, especially during the first two weeks of operation. Furthermore, most farmers produce potatoes during the month of June.

Figure 6 depicts the overall development of potatoes plants from first two months after plantation until the growth of the plant development ends. Our revised yielding modelling equation (17) has been used to produce Figure 6.

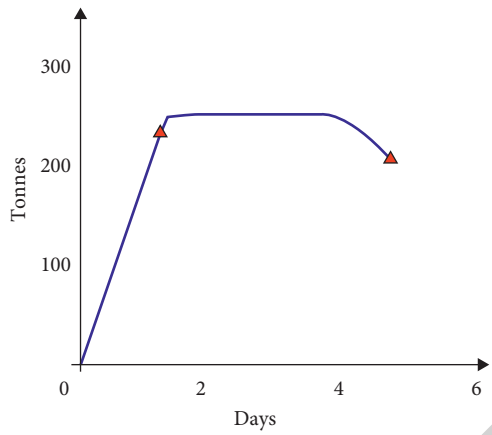

Figure 5: Progress of biomass graph for potato.

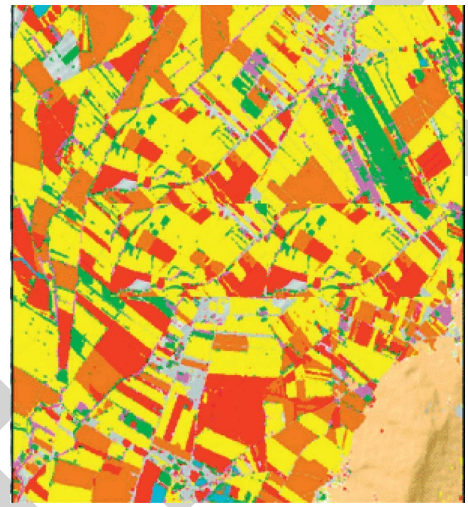

Figure 6: Crops in Bekaa Valley.

Table 4: Estimated biomass production for potato in 2020.

	15th March	20th April	16th May	23rd June	19th July
Days	2	26	27	39	46
Mean	0	0.7	36	116	40.2
Minimum	0	0.25	15	52	7.3
Maximum	0	2.5	70	142	79.2

$$\text{The factor of beginning data} = \beta_1 \exp\left(-\left(\frac{\text{beginning data} - y_1}{z_1}\right)^2\right) \times \beta_2 \exp\left(-\left(\frac{\text{beginning data} - y_2}{z_2}\right)^2\right),$$
$$\text{new biomass} = \sum_{j=1}^{M} \text{factor of beginning data}. \tag{17}$$

The novel agricultural production technique was used to produce graphic mapping as shown in Figure 6. This method creates the overall field pattern and the project above-ground biomass and plant weight that includes dried material content from potatoes. Actual biomass information was collected frequently from the potato farms during every

Table 5: Potato crop yields for numerous farms in Bekaa Valley's various locations.

List	Zone	Cultivation	Variety	Estimated in tonnes	Defects
Farmer 1	40	23	S	14.5	0.001
Farmer 2	45	26	S	16.2	0.003
Farmer 3	60	15	A	12.3	0.002
Farmer 4	75	14	S	33.2	0.002
Farmer 5	80	16	A	18	0.001

S: Spunta; A: Agria.

week after the planting date. Then, every ten days, the data were collected to verify the potato field map. As seen in this figure, the projected study agreed to 96.5 percent.

Many potato farmers were contacted to build trust for their predicted yielding rate. Table 4 displays both actual versus projected potato yields as per the information gathered and the proposed system. According to this report, the overall reliability for predicted agricultural yields was around 94 percent.

By terms of possessing real numbers larger than or similar to overall predicted levels, generally there was consistency among all information collected. The curve was typically equivalent or down to 80 percentage point of a potato weight, and this same information from Table 5 was consistent. This indicates that the verification procedure was accurate with completion for the proposed design. Furthermore, we could see how overall agricultural output across many areas was quite poor, which might be due to high level of farm modelling error.

7. Conclusion

The lack of information about remote sensing was not going to be a significant obstacle to agricultural management, including policy development. Crop yield prediction can be greatly improved with the intelligent monitoring system available to assist and remove obstacles that may arise during estimation. An intelligent system may decide to immediately calculate the agricultural production rate or to use other statistical methods to improve the overall availability of remote sensing information. The developed theoretical model was constructed from information available in nonlinear equations using the optimisation technique. Our research results showed that the accuracy of the remote sensing image, regardless of spatial resolution and poor quality, can be improved when calculating the crop yield rate. The potato crop estimation was executed correctly and the same was validated with the farmers in real time. The harvest was put in place to demonstrate the effectiveness of the survey. This was aimed at improving the proposed system by introducing additional elements that will support improved overall management of a broad range of agricultural activities. It will also help create different agricultural databases that could help decision makers find the solution to their needs.

Data Availability

The data shall be made available on request to the corresponding author.

Conflicts of Interest

The authors declare that they have no conflicts of interest.

References

[1] A. Roy and A. B. Inamdar, "Multi-temporal land use land cover (LULC) change analysis of a dry semi-arid river basin in western India following a robust multi-sensor satellite image calibration strategy," *Heliyon*, vol. 5, no. 4, Article ID e01478, 2019.

[2] A. Nemmaoui, M. A. Aguilar, F. J. Aguilar, A. Novelli, and A. García Lorca, "Greenhouse crop identification from multi-temporal multi-sensor satellite imagery using object-based approach: a case study from almería (Spain)," *Remote Sensing*, vol. 10, no. 11, p. 1751, 2018.

[3] A. Raghuvanshi, U. K. Singh, G. S. Sajja et al., "Intrusion detection using machine learning for risk mitigation in IoT-enabled smart irrigation in smart farming," *Journal of Food Quality*, vol. 2022, Article ID 3955514, 8 pages, 2022.

[4] V. Hemamalini, S. Rajarajeswari, S. Nachiyappan et al., "Food quality inspection and grading using efficient image segmentation and machine learning-based system," *Journal of Food Quality*, vol. 2022, Article ID 5262294, 6 pages, 2022.

[5] C. L. M. de Oliveira Santos, R. A. C. Lamparelli, G. K. Dantas Araújo Figueiredo et al., "Classification of crops, pastures, and tree plantations along the season with multi-sensor image time series in a subtropical agricultural region," *Remote Sensing*, vol. 11, no. 3, p. 334, 2019.

[6] B. Barrett, I. Nitze, S. Green, and F. Cawkwell, "Assessment of multi-temporal, multi-sensor radar and ancillary spatial data for grasslands monitoring in Ireland using machine learning approaches," *Remote Sensing of Environment*, vol. 152, pp. 109–124, 2014.

[7] S. M. Ghosh and M. D. Behera, "Aboveground biomass estimation using multi-sensor data synergy and machine learning algorithms in a dense tropical forest," *Applied Geography*, vol. 96, pp. 29–40, 2018.

[8] S. Chauhan, R. Darvishzadeh, M. Boschetti, and A. Nelson, "Estimation of crop angle of inclination for lodged wheat using multi-sensor SAR data," *Remote Sensing of Environment*, vol. 236, Article ID 111488, 2020.

[9] N. Zeng, H. He, X. Ren et al., "The utility of fusing multi-sensor data spatio-temporally in estimating grassland aboveground biomass in the three-river headwaters region of China," *International Journal of Remote Sensing*, vol. 41, no. 18, pp. 7068–7089, 2020.

[10] Z. Mashaba-Munghemezulu, G. J. Chirima, and C. Munghemezulu, "Mapping smallholder maize farms using multi-temporal sentinel-1 data in support of the sustainable development goals," *Remote Sensing*, vol. 13, no. 9, p. 1666, 2021.

[11] T. T. Nguyen, T. D. Pham, C. T. Nguyen et al., "A novel intelligence approach based active and ensemble learning for agricultural soil organic carbon prediction using multispectral and SAR data fusion," *Science of the Total Environment*, vol. 804, Article ID 150187, 2022.

[12] S. Hartling, V. Sagan, and M. Maimaitijiang, "Urban tree species classification using UAV-based multi-sensor data fusion and machine learning," *GIScience and Remote Sensing*, vol. 58, pp. 1–26, 2021.

[13] Z. Ji, Y. Pan, X. Zhu, J. Wang, and Q. Li, "Prediction of crop yield using phenological information extracted from remote sensing vegetation index," *Sensors*, vol. 21, no. 4, p. 1406, 2021.

[14] N.-T. Son, C.-F. Chen, C.-R. Chen et al., "Machine learning approaches for rice crop yield predictions using time-series satellite data in Taiwan," *International Journal of Remote Sensing*, vol. 41, no. 20, pp. 7868–7888, 2020.

[15] M. C. Anderson, Y. Yang, J. Xue et al., "Interoperability of ECOSTRESS and Landsat for mapping evapotranspiration time series at sub-field scales," *Remote Sensing of Environment*, vol. 252, Article ID 112189, 2021.

[16] L. A. Ebert, A. J. Chisholm, J. Prater et al., "How high to fly? evaluating different elevations for mapping evapotranspiration from remotely piloted aircrafts," in *Proceedings of the AGU Fall Meeting Abstracts*, vol. 2020, Chicago, IL, USA, 2020.

[17] A. Abdolghafoorian, "An integrated variational framework for mapping evapotranspiration by assimilating GOES LST and SMAP data," in *Proceedings of the EGU General Assembly Conference Abstracts*, Vienna, Austria, 2020.

[18] J. M. Ramírez-Cuesta, R. G. Allen, D. S. Intrigliolo et al., "METRIC-GIS: an advanced energy balance model for computing crop evapotranspiration in a GIS environment," *Environmental Modeling & Software*, vol. 131, Article ID 104770, 2020.

[19] M. Saboori, A. Mokhtari, Y. Afrasiabian, A. Daccache, S. Alaghmand, and Y. Mousivand, "Automatically selecting hot and cold pixels for satellite actual evapotranspiration estimation under different topographic and climatic conditions," *Agricultural Water Management*, vol. 248, Article ID 106763, 2021.

[20] J. Zhao, C. Li, T. Yang et al., "Estimation of high spatio-temporal resolution actual evapotranspiration by combining the SWH model with the METRIC model," *Journal of Hydrology*, vol. 586, Article ID 124883, 2020.

[21] H. Gacanin and M. Di Renzo, "Wireless 2.0: toward an intelligent radio environment empowered by reconfigurable meta-surfaces and artificial intelligence," *IEEE Vehicular Technology Magazine*, vol. 15, no. 4, pp. 74–82, 2020.

[22] P. Ratta, A. Kaur, S. Sharma, M. Shabaz, and G. Dhiman, "Application of blockchain and internet of things in healthcare and medical sector: applications, challenges, and future perspectives," in *Journal of Food Quality*, R. Khan, Ed., vol. 2021, Article ID 7608296, 20 pages, 2021.

[23] M. Knaus and D. Haase, "Green roof effects on daytime heat in a prefabricated residential neighbourhood in Berlin, Germany," *Urban Forestry and Urban Greening*, vol. 53, Article ID 126738, 2020.

[24] Z.-M. Wang, F.-H. Ren, D.-W. Luo, Z.-Y. Yan, and L.-A. Wu, "Almost-exact state transfer by leakage-elimination-operator control in a non-Markovian environment," *Physical Review A*, vol. 102, no. 4, Article ID 042406, 2020.

[25] S. A. Bassey, "Technology, environmental sustainability and the ethics of anthropoholism," in *Proceedings of the International Symposium for Environmental Science and Engineering Research (ISESER2020)*, p. 85, Manisa, Turkey, 2020.